Optics Letters

Dispersion-corrected frequency-resolved optical gating

Po-Ya Wu,[1] Hsuan-Hao Lu,[1] Ching-Zhe Weng,[1] Yen-Hung Chen,[2] and Shang-Da Yang[1,3,*]

[1]Institute of Photonics Technologies, National Tsing Hua University, Hsinchu 30013, Taiwan
[2]Department of Optics and Photonics, National Central University, Jhongli 320, Taiwan
[3]Department of Electrical Engineering, National Tsing Hua University, Hsinchu 30013, Taiwan
*Corresponding author: shangda@ee.nthu.edu.tw

Received 1 August 2016; revised 1 September 2016; accepted 1 September 2016; posted 1 September 2016 (Doc. ID 272912); published 27 September 2016

The phase retrieval algorithm of a frequency-resolved optical gating (FROG) is generalized to handle traces seriously distorted by group delay dispersion and non-uniform phase-matching spectra arising from the nonlinear crystal. In our proof-of-concept experiments, 15 mm thick aperiodically poled lithium niobate was employed in FROG, and successfully reconstructed chirped signal pulses were actually stretched by >5 times inside the crystal. This method is particularly promising in the measurement of weak few-cycle pulses produced by supercontinuum generation in fibers.

OCIS codes: (320.7100) Ultrafast measurements; (320.7110) Ultrafast nonlinear optics.

http://dx.doi.org/10.1364/OL.41.004538

Self-referenced femtosecond pulse measurement techniques typically rely on crystal nonlinearity to achieve temporal gating or spectral shearing. Since the nonlinear signal yield increases with the interaction length, it is desirable to employ thicker crystals in pulse measurement. Unfortunately, a thicker crystal results in a larger group velocity mismatch (GVM) walk-off [1], i.e., a narrower phase-matching (PM) bandwidth, and stronger fundamental pulse distortion caused by group delay dispersion (GDD) [2]. For techniques based on $\chi^{(2)}$ nonlinearity [e.g., second-harmonic (SH) generation], GVM walk-off is a tighter constraint on the upper bound of applicable crystal thickness $L_{\max}$, unless the test pulse width approaches one carrier cycle. This restriction has been overcome by using chirped quasi-phase matched (QPM) gratings [3] or novel measurement methods [4,5]. On the other hand, $\chi^{(3)}$-techniques (e.g., polarization gating) are less sensitive, though they are immune to the GVM issue. In either case, $L_{\max}$ is still limited by GDD to date. To show how serious this problem could be, we used five power spectra [Fig. 1(a)] reported in the multi-plate continuum experiment [6] to calculate the corresponding transform-limited (TL) pulse widths Δt_{TL} and the output pulse widths $\Delta t'$ after these TL pulses pass through different Type I BBO crystal thicknesses L. The maximum crystal thickness $L_{\max}$ in Fig. 1(b) is defined by the L value at which $\Delta t' = 1.05\Delta t_{\mathrm{TL}}$ occurs. The simulation results show that $L_{\max}$ rapidly drops by 170 folds (from 1.7 mm to 10 μm), as Δt_{TL} decreases by 10 times (from 23 to 2.3 fs).

In this Letter, we generalize the phase retrieval algorithm of frequency-resolved optical gating (FROG) [7] to deal with traces seriously distorted by GDD and the non-uniform PM spectral response [3] via guaranteed convergence particle swarm optimization (GCPSO) [8]. The elimination of the crystal thickness constraint would not only ease the choice of nonlinear crystal, but also would multiply the sensitivity in measuring weak few-cycle pulses.

The SH spectrum $E_2(\Omega)$ due to pulse replicas of individual spectral envelope $E_1(\omega')$ and time delay τ passing through a nonlinear crystal of length L is formulated as [9]

$$E_2(\Omega,\tau,L) \propto \left\{\left[\frac{-j\cdot\Omega}{2\cdot n_{2\omega}(\Omega)\cdot c_0}\right]\times\exp[-j\cdot k_{2\omega}(\Omega)\cdot L]\right\} \times\left\{\int_0^{\infty} E_1(\omega')\times\exp(-j\cdot\omega'\cdot\tau)\times E_1(\Omega-\omega') \times\left[\int_0^{L} d_{\mathrm{eff}}(z)\times\exp(j\cdot\Delta k\cdot z)\mathrm{d}z\right]\mathrm{d}\omega'\right\}, \quad (1)$$

where $d_{\mathrm{eff}}(z)$ is the effective nonlinear coefficient distribution, and Δk is the wave vector mismatch term defined as

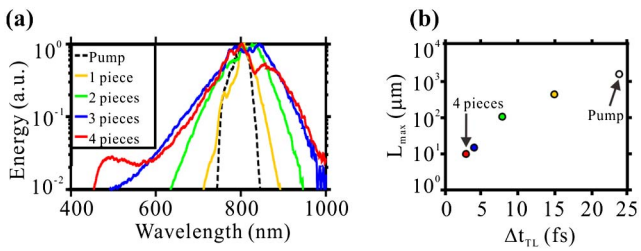

Fig. 1. (a) Power spectra of the pump pulse (dashed) and those after passing through different numbers of strategically placed 100 μm thick fused silica plates [6]. (b) Maximum BBO crystal length $L_{\max}$ (defined in the main text) versus the input TL pulse width Δt_{TL}.

$$\Delta k(\Omega, \omega') \equiv k_{2\omega}(\Omega) - k_{\omega}(\omega') - k_{\omega}(\Omega - \omega'). \quad (2)$$

In the presence of weak GDD, Δk reduces to a function of Ω, and Eq. (1) is simplified as a transfer function relation:

$$E_2(\Omega, \tau, L) \propto F(\Omega) \times H(\Omega), \quad (3)$$

where

$$F(\Omega, \tau) \propto \int_0^{\infty} E_1(\omega') \times e^{-j\omega'\tau} \times E_1(\Omega - \omega')\mathrm{d}\omega', \quad (4)$$

$$H(\Omega) \propto \exp[-j \cdot k_{2\omega}(\Omega) \cdot L] \times \int_0^{L} d_{\mathrm{eff}}(z) \times \exp(j \cdot \Delta k \cdot z)\mathrm{d}z \quad (5)$$

are the nonlinear polarization spectral envelope and the PM spectrum contributed by the crystal, respectively. Standard phase retrieval algorithms of SHG FROG apply if the trace formula $I_{\mathrm{FROG}}(\Omega, \tau) \propto |F(\Omega, \tau)|^2$ holds [under negligible GDD and flat $H(\Omega)$], which is untrue when using a long, chirped QPM grating [3].

The proposed dispersion-corrected (DC) FROG works as follows. (i) We create a pool of M vectors $\vec{\psi}_m(n)(m = 1, 2, \ldots, M; n = 1, 2, \ldots, N)$ to represent M possible spectral phase functions. Each is sampled at N frequencies. In all of our simulations, $M = 5$ and $N = 10$ are used. (ii) Since the given power spectrum $|E_1(\omega)|^2$ is sampled at $N_i(> N)$ frequencies, M spectral phase functions (thus, M complex fields) of the same resolution are obtained by interpolating $\{\vec{\psi}_m(n)\}$. (iii) The double integral formula Eq. (1) is used in calculating M FROG traces (of grid size $N_i \times N_i$) for the given combination of fundamental fields $E_1(\omega)$ and a nonlinear crystal structure $d_{\mathrm{eff}}(z)$. (iv) The fitness of $\vec{\psi}_m(n)$ is quantitatively evaluated by the FROG error between the measured and calculated FROG traces $I_{\mathrm{FROG}}^{(\mathrm{exp})}$ and $I_{\mathrm{FROG}}(\vec{\psi}_m)$:

$$\epsilon(\vec{\psi}_m) = \sqrt{\frac{1}{N_i^2}\sum_{\Omega,\tau}[I_{\mathrm{FROG}}^{(\mathrm{exp})} - I_{\mathrm{FROG}}(\vec{\psi}_m)]^2},$$

and the pool is updated by minimizing ϵ via GCPSO.

In particle swarm optimization (PSO), a possible $\vec{\psi}_m(n)$ is treated as a "particle" and moves around in the N-dimensional problem space in search of the extremum iteratively. The displacement (distance and direction) of each particle depends on its own inertia (i.e., tendency to retain the original moving behavior), the personal history of previous displacements, and the history of the entire swarm [10]. GCPSO prevents local minimum traps by introducing an additional particle to search randomly around the current best solution.

DC FROG differs from the standard FROG in two major aspects. (i) A gated signal is calculated by Eq. (1), instead of Eq. (3). (ii) In each iteration, a better solution is approached by updating the entire vector pool according to the particle displacement rules of GCPSO (without using $I_{\mathrm{FROG}}^{(\mathrm{exp})}$). In contrast, a standard FROG relies on replacing the gated spectral intensity by $I_{\mathrm{FROG}}^{(\mathrm{exp})}$ to approach the spectral phase.

The DC FROG was numerically verified as follows. The test pulses were created by combining a power spectrum supporting a 28-fs TL pulse at ~800 nm [shaded, Fig. 2(a)] and two types of spectral phase curves, including a cubic function ψ_1 [solid, Fig. 2(a)] and a sinusoidal function ψ_2 [solid, Fig. 2(e)], respectively. The corresponding temporal intensities $I_1(t)$ and $I_2(t)$ exhibit deep modulation [solid, Figs. 2(b) and 2(f)], which are nontrivial for reconstruction. The ideal FROG traces arising from an extremely thin crystal (with a negligible GDD and flat PM response) were calculated by the modulus square of Eq. (4) [Figs. 2(c) and 2(g)]. The impacts of crystal dispersion were numerically analyzed by assuming a 15 mm long 5 mol% MgO-doped aperiodically poled lithium niobate (APPLN) with QPM periods linearly chirped from 9.016 to 16.595 μm, which is long enough to significantly stretch and distort the input pulses [insets, Figs. 2(b) and 2(f)], while preserving a sufficiently broad PM bandwidth (364–430 nm at the SH band). The resulting FROG traces calculated by the modulus square of Eq. (1) [left panels, Figs. 2(d) and 2(h)] greatly differ from their ideal counterparts [Figs. 2(c) and 2(g)], implying that no reliable solution can be obtained by traditional FROG

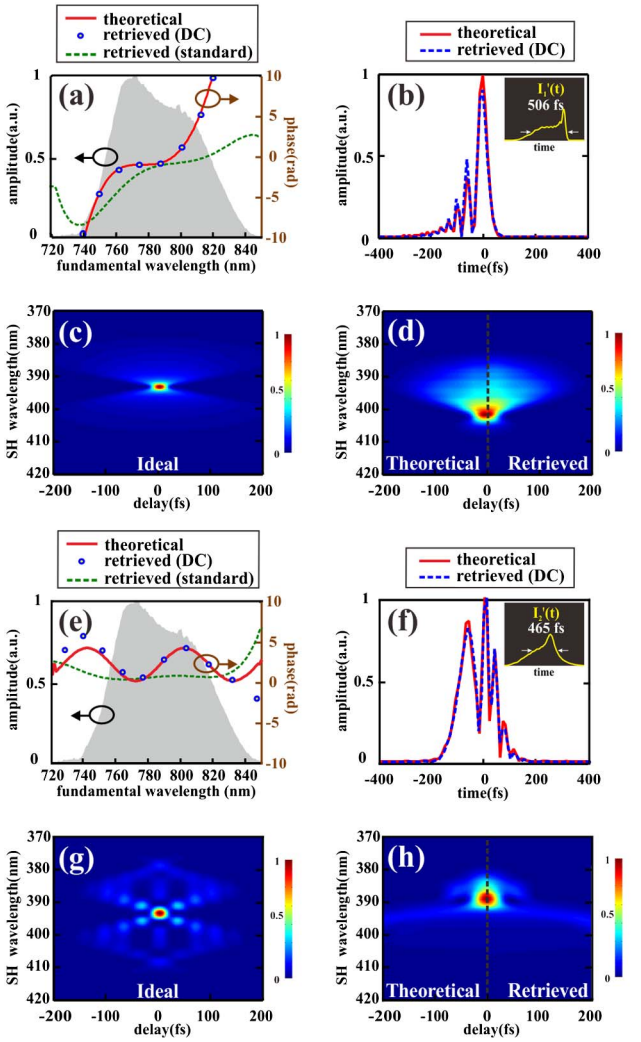

Fig. 2. (a) Power spectrum (shaded) and spectral phase function ψ_1 obtained by assumption (solid) and numerical retrieval using DC FROG (circles) and standard FROG (dashed), respectively. (b) Assumed (solid) and retrieved (dashed) temporal intensities $I_1(t)$ of the test pulse. The inset shows the temporal intensity $I_1'(t)$ distorted by a 15 mm long APPLN. (c) Ideal theoretical SHG FROG trace for a zero-thickness crystal. (d) FROG traces distorted by a 15 mm long APPLN before (left) and after (right) the GCPSO reconstruction. (e)–(h) Counterparts of (a)–(d) for a sinusoidal spectral phase function ψ_2.

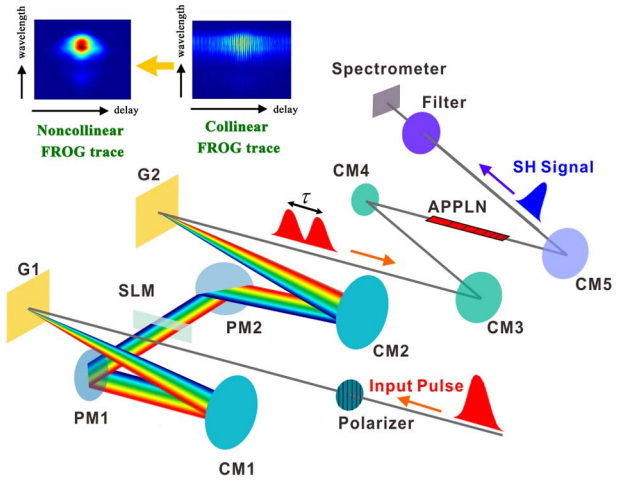

Fig. 3. Experimental setup. [CM#, concave mirror; G#, grating; PM#, plane mirror; SLM, spatial light modulator.]

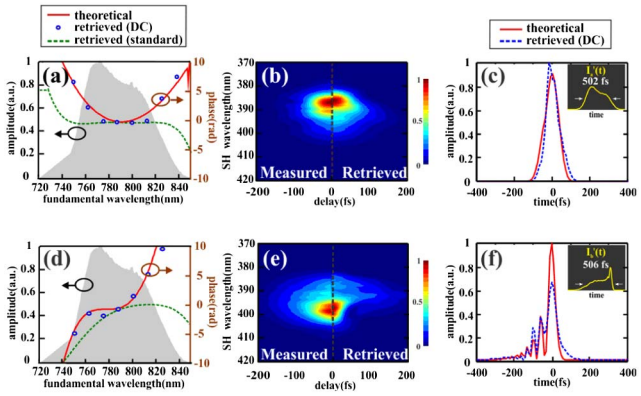

Fig. 4. (a) Experimental power spectrum (shaded) and spectral phase function ψ_a applied by the pulse shaper (solid) and obtained by numerical retrieval using DC FROG (circles) and standard FROG (dashed), respectively. (b) FROG traces distorted by a 15 mm long APPLN before (left) and after (right) the GCPSO reconstruction. (c) Assumed (solid) and retrieved (dashed) temporal intensities $I_a(t)$ of the test pulse. The inset shows the temporal intensity $I'_a(t)$ distorted by a 15 mm long APPLN. (d)–(f) Counterparts of (a)–(c) for a cubic spectral phase function ψ_b.

algorithms. However, a DC FROG with a built-in GCPSO process can still converge to the distorted FROG traces [right panels, Figs. 2(d) and 2(h)] with very low FROG errors (2.8×10^{-4} and 3.0×10^{-5}). The retrieved spectral phase functions [circles, Figs. 2(a) and 2(e)] and temporal intensities [dashed, Figs. 2(b) and 2(f)] are in good agreement with the assumed ones, even in the presence of the serious crystal dispersion.

Figure 3 shows the setup used in our proof-of-concept experiments. The light source is a Ti:sapphire amplifier (FEMTOPOWER compact PRO, Femtolasers), producing 1 kHz, ~30 fs pulses at ~800 nm. A Fourier transform pulse shaper [11] made of gratings (G1 and G2, 200 grooves/mm), concave mirrors (CM1 and CM2, $f = 200$ mm), plane mirrors (PM1 and PM2), and a spatial light modulator (SLM, SLM-128-D-VN, CRi) replaces the typical Michelson interferometer [12,13] because of a couple of practical merits. (i) No broadband beam splitter is required, which would be a strategic advantage in octave-spanning signal characterizations. (ii) High-precision (down to sub-attosecond) delays can be created by programming the SLM driving voltages [14]. (iii) The average fringe density of an interferometric SH trace can be reduced by controlling the carrier-envelope phase without compromising the fidelity of the pulse reconstruction. The down-sampling functionality enables either a shorter data acquisition time or a higher measurement sensitivity [13]. (iv) The residual spectral phase arising from the air path or the optical elements can be pre-compensated for. The optical beam is reduced below 1 mm in diameter by two concave mirrors CM3 ($f = 100$ mm) and CM4 ($f = 9.5$ mm), passing through the APPLN (15 mm × 2 mm × 1 mm) with linearly chirped poling periods ranging from 9.016 to 16.595 μm. The 15 mm crystal length is sufficient to broaden the TL input pulse by >14 times, while the range of poling periods prevents spectral truncation at the SH band. The SH signal pulse is focused into a spectrometer (USB2000+, Ocean Optics) by a concave mirror (CM5) for power spectral acquisition at different delays. The raw data (collinear FROG trace) have to be post-processed [15] such that a non-collinear trace without delay fringes and signal background can be fed to the DC FROG algorithm.

Figure 4 shows two sets of experimental results. The two test pulses were created by the same power spectrum [shaded, Figs. 4(a) and 4(d)] and different spectral phase functions $\psi_a = (6.3246 \times 10^2\ \text{fs}^2/\text{rad}) \times (\omega - \omega_0)^2/2$ [solid, Fig. 4(a)] and $\psi_b = (-2.846 \times 10^4\ \text{fs}^3/\text{rad}^2) \times (\omega - \omega_0)^3/6$ [solid, Fig. 4(d)] via the pulse shaper, respectively ($\omega_0 = 2\pi \times 381$ THz). Although the non-collinear FROG traces before and after the iterative reconstruction of the DC FROG exhibit a certain discrepancy [left and right panels, Figs. 4(b) and 4(e)], the retrieved spectral phase functions [circles, Figs. 4(a) and 4(d)] and temporal intensities [dashed, Figs. 4(c) and 4(f)] remain in good agreement with the assumed counterparts [solid, Figs. 4(a), 4(c), 4(d), 4(f)]. The corresponding FROG errors are 3.0×10^{-4} [Fig. 4(b)] and 5.6×10^{-4} [Fig. 4(e)]. In contrast, standard FROG essentially fails to recover the spectral phases [dashed, Figs. 4(a) and 4(d)].

The accuracy in these preliminary tests is primarily limited by some technical issues. (i) To create a larger delay, the pulse shaper needs to apply a denser spectral cosine modulation. Since our pulse shaper (designed for an octave-spanning spectrum) has a spectral resolution of ~2.32 THz, the maximum delay (~430 fs) might not be sufficient to accurately split the test pulses into two isolated replicas. This explains why the second test pulse with a wider temporal spreading [solid, Fig. 4(f)] is subject to a larger measurement error. (ii) The dispersion relation of the actually used crystal might differ from the Sellmeier equation with reported parameters. In fact, there is noticeable uncertainty among the reported Sellmeier equation parameters for 5 mol. % MgO-doped $LiNbO_3$ [16,17]. (iii) The actual $d_{\text{eff}}(z)$ of the APPLN could be inconsistent with the designed one due to fabrication errors. These technical issues can be solved by improving the spectral resolution of the pulse shaper (using a larger beam size, a longer focal length, and more SLM pixels), the accuracy of the crystal dispersion (performing white-light interferometry measurement), and the experimental diagnosis of the domain orientation function [18].

In conclusion, we have demonstrated a new DC FROG algorithm based on the more complete double-integral SHG formalism and the GCPSO optimization process, which is applicable to FROG traces considerably distorted by GDD and the non-uniform PM spectral response. In our proof-of-concept experiments, Ti:sapphire amplifier pulses with quadratic and cubic spectral phases were successfully characterized by using a 15 mm thick APPLN (sufficient to broaden the test pulses from <100 fs to >500 fs in duration) and the DC FROG algorithm. The precision of the DC FROG reconstruction is currently subjected to some technical issues, which can be solved by improving the resolution of the pulse shaper and the accuracy of the APPLN parameters, and increasing the numbers of particles M and samplings N in the GCPSO algorithm. To the best of our knowledge, this is the first method fundamentally relaxing the dispersion limit imposed on nonlinear optical pulse measurement techniques. It enables the employment of long APPLN waveguides in measuring few-cycle pulses, which is expected to have unprecedented sensitivities.

Funding. Ministry of Science and Technology, Taiwan (MOST) (104-2112-M-007-012-MY3, 104-2218-E-007-004); National Tsing Hua University (NTHU) (104N2081E1).

Acknowledgment. The authors thank the Frontier Photonics Research Laboratory for the use of their equipment.

REFERENCES

1. A. M. Weiner, IEEE J. Quantum Electron. **19**, 1276 (1983).
2. X. S. Xiao, C. X. Yang, S. M. Gao, and H. X. Miao, IEEE J. Quantum Electron. **41**, 85 (2005).
3. S. D. Yang, H. Miao, Z. Jiang, A. M. Weiner, K. R. Parameswaran, and M. M. Fejer, Appl. Opt. **46**, 6759 (2007).
4. S. D. Yang, C. S. Hsu, S. L. Lin, H. Miao, C. B. Huang, and A. M. Weiner, Opt. Express **16**, 20617 (2008).
5. C. S. Hsu, Y. H. Lee, A. Yabushita, T. Kobayashi, and S. D. Yang, Opt. Lett. **36**, 2041 (2011).
6. C. H. Lu, Y. J. Tsou, H. Y. Chen, B. H. Chen, Y. C. Cheng, S. D. Yang, M. C. Chen, C. C. Hsu, and A. H. Kung, Optica **1**, 400 (2014).
7. R. Trebino, *Frequency-Resolved Optical Gating: The Measurement of Ultrashort Laser Pulses* (Kluwer Academic, 2002).
8. M. Clerc and J. Kennedy, IEEE Trans. Evol. Comput. **6**, 58 (2002).
9. A. M. Weiner, *Ultrafast Optics*, Pure and Applied Optics (Wiley, 2009).
10. Z. Cui and J. Zeng, *Rough Sets and Current Trends in Computing* (Springer, 2004), pp. 762–767.
11. A. M. Weiner, Rev. Sci. Instrum. **71**, 1929 (2000).
12. A. Galler and T. Feurer, Appl. Phys. B **90**, 427 (2008).
13. C. S. Hsu, H. C. Chiang, H. P. Chuang, C. B. Huang, and S. D. Yang, Opt. Lett. **36**, 2611 (2011).
14. J. Köhler, M. Wollenhaupt, T. Bayer, C. Sarpe, and T. Baumert, Opt. Express **19**, 11638 (2011).
15. G. Stibenz and G. Steinmeyer, IEEE J. Sel. Top. Quantum Electron. **12**, 286 (2006).
16. P. Brand, B. Boulanger, P. Segonds, Y. Petit, C. Félix, B. Ménaert, T. Taira, and H. Ishizuki, Opt. Lett. **34**, 2578 (2009).
17. O. Gayer, Z. Sacks, E. Galun, and A. Arie, Appl. Phys. B **91**, 343 (2008).
18. C. L. Tsai, M. C. Chen, J. Y. Lai, D. Y. Wu, and S. D. Yang, Opt. Express **21**, 11763 (2013).